2015 ASIA-PACIFIC SOLAR RESEARCH CONFERENCE

Peer Reviewed
2015 Solar Research Conference

Daniel Potter

Optimised Design of a 1 MW_t Liquid Sodium Central Receiver System

Daniel Potter[1], Alex Burton[1] and Jin-Soo Kim[1]

[1]CSIRO Energy, PO Box 330, Newcastle, NSW 2300, Australia

E-mail: daniel.potter@csiro.au

Abstract

An integrated computational model for optical and thermal analysis of central receiver systems was applied to optimise the field layout and receiver geometry for a $1MW_t$ liquid sodium cavity. Optimised polar field layouts were found by allowing heliostats to move on a annual performance based 'potential surface' balanced by shading and blocking induced 'collisions' until an equilibrium arrangement was attained. Aperture radius and aperture orientation were parametrically varied to determine an optimal arrangement. Detailed heat transfer calculations for a design point condition were used to verify the aperture radius selection and determine an optimal cavity depth. The thermal efficiency of the optimized receiver design at the design point was calculated to be 91.6%.

Nomenclature

α_c	Ambient air convective heat transfer coefficient (W/m2/K)	σ	Slope and tracking error (mrad)
α_f	Heat transfer fluid convective heat transfer coefficient (W/m^2/K)	r_a	Aperture radius (m)
A	Area (m^2)	r_c	Cavity radius (m)
η	Efficiency (%)	s	Facet side length (m)
ε_s	Solar emittance (-)	t	Wall thickness (m)
f	Surface-to-surface radiative exchange factor (-)	T_a	Ambient air temperature (K)
h_c	Cavity height (m)	T_f	Heat transfer fluid temperature (K)
k_w	Wall thermal conductivity (W/m/K)	T_w	Surface temperature (K)
l	Distance (m)	x	East-west coordinate (m)
P	Power output (kW)	y	North-south coordinate (m)
q_s	Solar irradiance (W/m2)	**Subscripts**	
σ_{lim}	Material strength limit (Pa)	e	External wall
σ_{VM}	von Mises Stress (Pa)	i,j,k	Surface facet and pipe element indices

1. Introduction

Central receiver concentrating solar thermal power plants are a promising clean and renewable alternative to fossil fuel power plants. Current state-of-the-art commercial facilities typically implement the tubular receiver concept where a flow of molten nitrate salt is heated to approximately 565°C to drive subcritical steam Rankine cycles with cycle efficiency of around 40%. The use of alternative heat transfer fluids such as liquid sodium may allow access to higher efficiency power cycles such as the supercritical CO_2 Brayton cycles, which have been predicted to allow efficiencies in excess of 47% (Padilla et al., 2015). The increased turbine inlet temperature, however, requires the heat transfer fluid to operate at higher temperatures, thereby increasing thermal losses. Enclosing the receiver surface in a cavity can reduce these losses, however the aperture restricts the aiming strategy and positioning of the heliostats. The optimised design of central receiver systems targeting high temperature power cycles requires an integrated model of the field and receiver that considers both optical and thermal performance in a coupled manner.

The CSIRO is developing an integrated computational model for the coupled optical and thermal optimisation of central receiver systems. The model is based around a surface mesh description of the heliostats, receiver components and shading objects. Heliostat performance, solar irradiance maps and surface-to-surface radiation transfer exchange factors are calculated via a dual band Monte-Carlo ray tracing model. This ray tracing model has been used successfully in previous work to aid receiver design (Kim et al., 2013). The thermal performance of the receiver is simulated by solving the system of nonlinear equations describing a steady state energy balance. Natural and forced convective cooling is modelled by loose coupling with an OpenFOAM Navier-Stokes solver. In this work, the integrated model is applied optimize the heliostat field layout and receiver geometry for a 1 MW_t liquid sodium central receiver system.

2. Problem description

The design parameters for the central receiver system to be optimised are specified in Table 1. The location has been selected to be Perenjori in Western Australia, as the high insolation and significant industry in the local area make it a realistic site for a CSP facility for electricity production. As the downstream plant (e.g. thermal storage and power cycle) is not modelled in this study, the facility performance requirement is given in terms of thermal energy and power output from the receiver. The annual thermal energy output is to be no less than 2500 MWh, with a maximum thermal power output of 1 MW. A number of such systems could be combined in a modular fashion to provide thermal energy input for a commercial scale turbine. The receiver is specified to be a tubular type with liquid sodium as the heat transfer fluid, and the cavity is constrained to a PS10 like geometry with a circular aperture, Figure 1, with two independent centre-to-side flow paths. The receiver inlet and outlet temperatures are set at 500°C and 700°C, respectively, which are selected based on a supercritical CO_2 Brayton cycle without thermal storage. As the path length and therefore also the pressure drop is anticipated to be low, a receiver pipe with both a small diameter and wall thickness is preferable. The NPS1/8 SCH5s receiver pipes are to be fabricated from Haynes® 230® Alloy with a Pyromark®2500 coating, where the solar reflectance and thermal emittance are assumed to be 0.05 and 0.85 respectively (Ho et al., 2013). The receiver pipes are to be arranged in banks of 15 pipes connected by headers at the inlet and outlet, with 4 banks per panel and therefore 8 banks per flow path. The facility parameters open to optimisation are the heliostat field layout, aperture radius, aperture orientation, cavity radius and cavity height.

Table 1 Specified facility constraints.

Location	Perenjori, Western Australia (-29.443, 116.285)
Annual energy output	2500 MWh
Max thermal power output	1 MW
Receiver type	PS10-like cavity (see Figure 1)
Heat transfer fluid	Liquid sodium
Inlet and output temperatures	500°C & 700°C
Receiver pipe size	NPS1/8 SCH5s
Receiver pipe material	Haynes® 230® Alloy
Receiver pipe coating	Pyromark®2500
Insulation material	Fibrefrax® Durablanket (128 kg/m^3)
Insulation thickness	300 mm
Heliostat type	CSIRO 2.25 m × 2.25 m single facet heliostat
Tower height	30 m

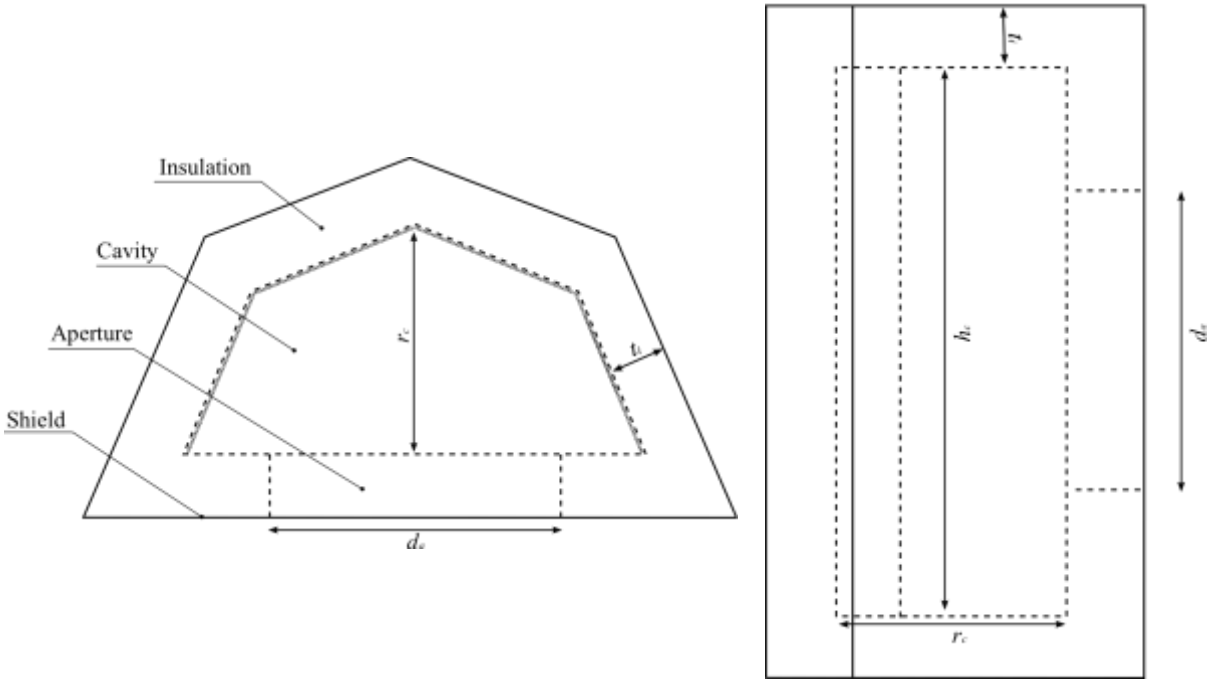

(a) Top view (b) Side view

Figure 1: Illustration of cavity receiver geometry.

3. Physical modeling

An integrated model for optical and heat transfer analysis of central receiver systems has been developed, Figure 2. The core components of the model are a Monte Carlo ray tracer and a

steady state heat transfer model. All objects contributing to the optical and thermal performance of the facility (e.g. heliostats, receiver and other shading objects such as buildings) are described by 2D surface meshes. The 3D CAD and mesh generation software SALOME Platform is used to create both a 2D surface mesh and 3D surrounding mesh for a representation of the receiver geometry. The 3D mesh is used for accurate determination of convective cooling by loose coupling of the steady state energy balance equations with an OpenFOAM Navier-Stokes solver.

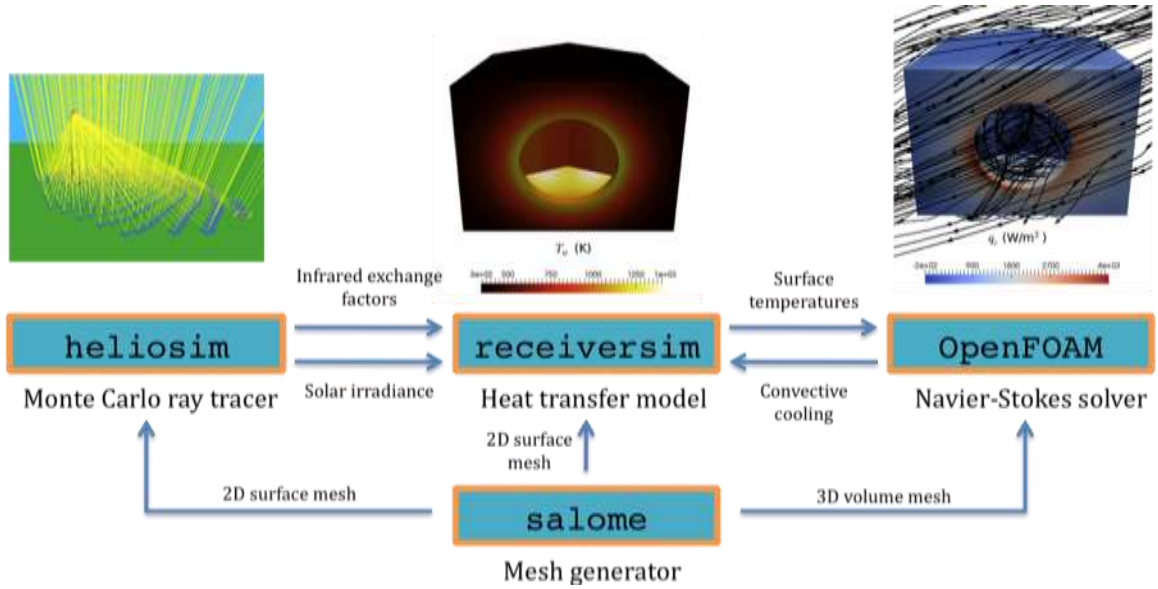

Figure 2: Components of the integrated central receiver system model, and their interactions.

3.1. Monte Carlo ray tracing

Optical performance of the heliostat field, solar irradiance distributions on the receiver and surface-to-surface thermal radiation exchange factors are computed by a Monte Carlo ray tracing model. For the solar radiation transport calculation, rays are cast from mirror surfaces rather than the sun, significantly improving computational efficiency. Shading and blocking is determined by tracing a minimal number of rays towards the sun. The directional probability distribution of rays reflected from the mirror surfaces is then calculated by convolving the sun shape with the slope and tracking error, Figure 3. This results in a degraded sun shape that incorporates the slope and error of the mirrors, Figure 4.

Rays cast from mirror surface facets that are not shaded or blocked are then propagated into the scene and allowed to interact with the modelled receiver components (pipe panels, insulation, shielding etc) according to the mean solar weighted diffuse reflectances and absorptances of the surfaces. Similarly, in order to compute surface-to-surface thermal radiation exchange factors, rays representing diffuse emission are cast from all facets describing the receiver components according to the mean infrared weighted diffuse reflectances and absorptances of the surfaces. The rate of reflection and absorption are treated non-probabilistically according to the energy partitioned method (Modest, 2013), where rays progressively loose energy upon surface interactions until depleted. The direction of diffusely reflected or emitted rays is treated probabilistically using the standard Monte Carlo relations. Due to the relatively small size of the field considered in the present work, attenuation of solar

radiation due to absorption and scattering by the atmosphere between the heliostats and receiver is not considered.

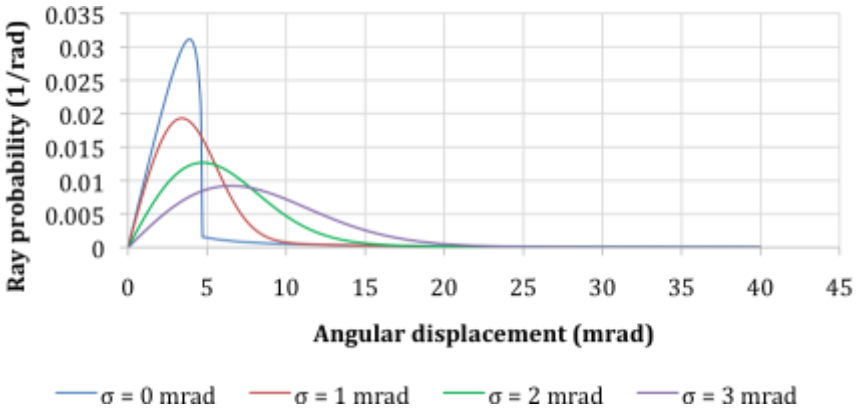

Figure 3: Directional probability distribution of reflected rays for a range of mirror slope and tracking errors (σ).

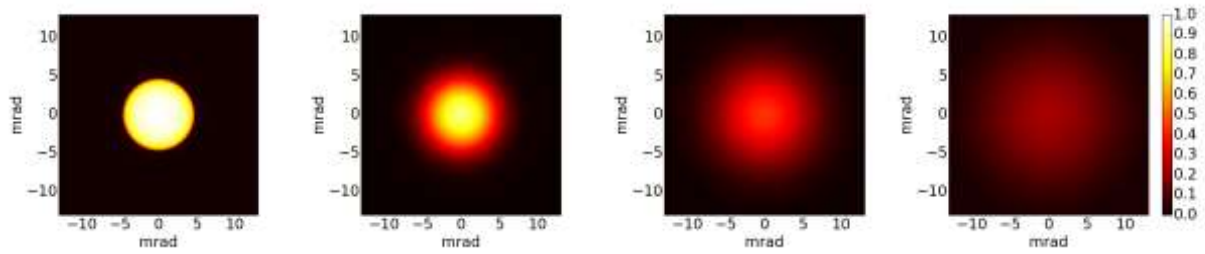

(a) σ = 0 mrad (b) σ = 1 mrad (c) σ = 2 mrad (d) σ =3 mrad

Figure 4: Normalised solar irradiance of degraded sun shapes for a range of mirror slope and tracking errors (σ).

3.2. Heat transfer

The computational domain for thermal analysis of the receiver consists of a simplified surface mesh (e.g. see **Error! Reference source not found.**a) with a one dimensional fluid network mesh mapped behind it and a three dimensional ambient air volume mesh mapped on top of it. In the present work, banks of receiver pipes are represented as flat surfaces. A system of nonlinear equations is created by considering the steady state energy balance for each surface facet in the computational domain:

$$\begin{aligned} 0 = A_i \bar{\epsilon}_{\mathrm{s},i} q_{\mathrm{s},i} \quad &+ \quad \sum_{j}^{N_s} f_{j,i} A_j \bar{\epsilon}_{\mathrm{t},j} \sigma T_{\mathrm{w},j}^4 - A_i \bar{\epsilon}_{\mathrm{t},i} \sigma T_{\mathrm{w},i}^4 - A_i \alpha_{\mathrm{c},i} \left(T_{\mathrm{w},i} - T_{\mathrm{a}} \right) \\ &+ \quad \sum_{j}^{N_{\mathrm{w_{adj.}}}} t_i s_{i,j} k_{\mathrm{w}} \frac{T_{\mathrm{w},j} - T_{\mathrm{w},i}}{\Delta l_{i,j}} + A_i k_{\mathrm{w}} \frac{\overline{T}_{\mathrm{w},e} - T_{\mathrm{w},i}}{t_i} \\ &- \quad \sum_{k}^{N_{p \in i}} \pi \Delta l_k \frac{k_{\mathrm{w}} \left(T_{\mathrm{w_o},i} - T_{\mathrm{f},k} \right)}{\ln \left(\frac{r_{\mathrm{o}}}{r_{\mathrm{i}}} \right) + \frac{1}{r_{\mathrm{i}}} \frac{k_{\mathrm{w}}}{\alpha_{\mathrm{f},i}}} \end{aligned} \tag{1}$$

For a given estimation of the surface temperature solution, the radial heat conduction into the heat transfer fluid at the fluid inlet where the fluid temperature is known can be calculated, and subsequently the mass, momentum and energy balance equations for internal pipe flow can be solved in a space marching fashion. This allows the rate of energy flow into the heat transfer fluid from each surface facet to be calculated. Similarly, for a given surface temperature solution, an estimation of the convective cooling due to ambient air flow can be obtained by running an OpenFOAM simulation with a constant temperature boundary condition. Thus the system of N_s energy balance equations (Equation 1) can be solved in terms of the set N_s surface temperatures via an iterative method.

In the present work the Nusselt number correlations proposed by Sleicher and Rouse (1975) are used on account of the low Prandtl number of the liquid sodium heat transfer fluid. Non-uniform mass flow rates in parallel flow paths (i.e. in pipes within a bank connected by headers at the inlet and outlet) are accounted for by ensuring the pressures of recombining flow paths are equal. Convective heat transfer is calculated via loose coupling with "buoyantSimpleFoam", the steady state Navier-Stokes solver for buoyant compressible fluid flows that is available in version 2.3.0 of OpenFOAM.

4. Field and aperture optimisation

The field layout was optimised by a crystallisation analogy combining two processes:

1. random motion of the heliostats on a 'potential surface' defined by annual performance of the possible layout space, and
2. 'collisions' when two heliostats interfered with each other through shading and blocking.

Combining these two processes for a given heliostat field layout allows a new and potentially improved improved layout to be obtained. This procedure is cycled many times until an equilibrium arrangement of the heliostats is achieved, Figure 5.

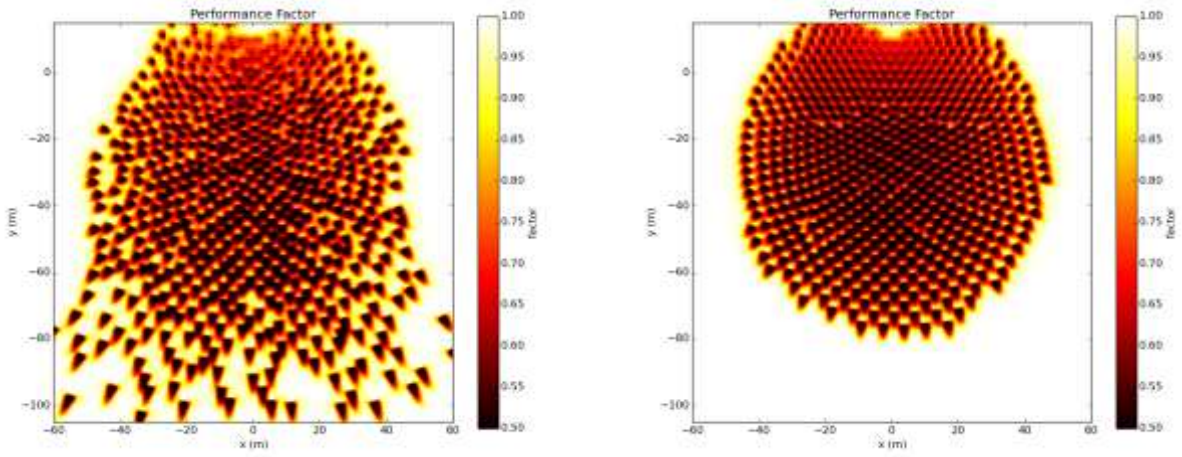

(a) 2000 iterations (b) 200000 iterations

Figure 5: Evolution of the heliostat field layout during optimisation to maximise annual performance (r_a=55 cm, θ_a=60, h_t=30 m), visualised with shading and blocking performance factor contours.

The calculation of annual thermal efficiency is made tractable by only performing ray tracing for 90 discrete solar positions (i.e. a Cartesian grid with 16 hour angle divisions and 5 declination divisions), and using a simplified model for receiver efficiency. For the optimization performed in the present work, 600 heliostats were allowed to find an optimal configuration in rectangular layout space spanning 15 m north, 105 m south and 60 m east and west of the tower. The minimum set of heliostats required to achieve the design requirement of 2500 MWh annual thermal output was then determined. This field optimisation procedure was performed for a number of possible aperture radii and orientation combinations, the results of which are summarised in Figure 6. The optimal combination is seen to be an aperture radii of 55 cm and optimal aperture orientation of 60° down from the horizon. The initial optimised layout of the 600 heliostats and the final reduced 413 heliostat layout are shown in Figure 7a and Figure 7b, respectively.

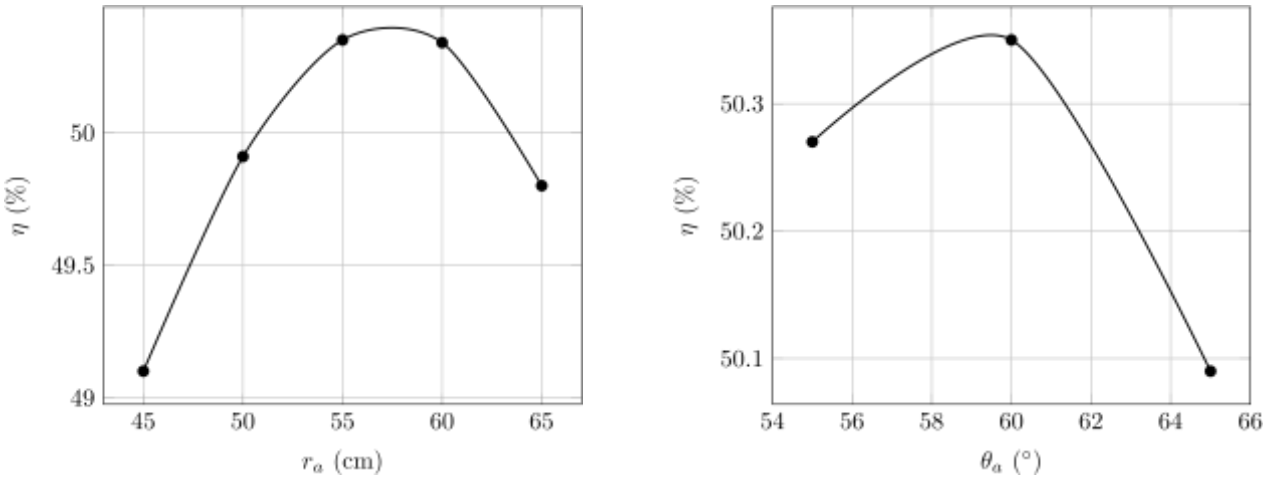

(a) Aperture radius (θ=60°, h=30 m) (b) Aperture angle (r=55 cm, h=30 m)

Figure 6: Sensitivity of annual thermal efficiency to aperture and tower parameters.

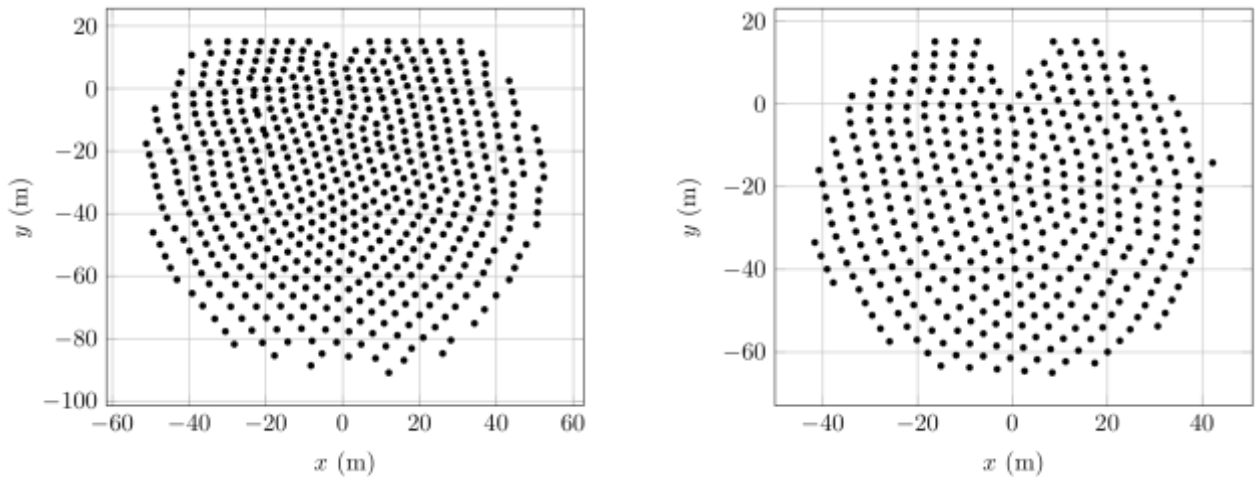

(a) Initial 600 heliostat layout (b) Reduced 413 heliostat layout

Figure 7: Optimised heliostat layout for best aperture setup (r=55 cm, θ=60°, h=30 m).

5. Receiver optimisation

Heat transfer simulations were performed using the optimised field (Figure 7b) for a design point condition to determine the optimal receiver geometry. The design point selected was solar noon on the Spring equinox (DNI=1002 W/m^2, wind = 1.6 m/s WNW, T_a=21°C). Figure 8 presents the sensitivity of receiver performance at the design point for various cavity radii. A receiver radii of 82.5 cm is seen to maximise the receiver efficiency, whilst maintaining a von Mises stress[1] in the pipe wall below the temperature dependent limit for Haynes 230 alloy specified by the ASME boiler code. The stresses in the pipe wall are estimated as the sum of the contributions due to pressure and temperature gradients between the outside and inside of the tube. For pressure stresses the standard pressure vessel relations are used, whilst for temperature induced stresses an empirical relation for a long circular cylinder with circumferentially uniform inner and outer wall temperatures is used (Timoshenko and Goodier, 1951).

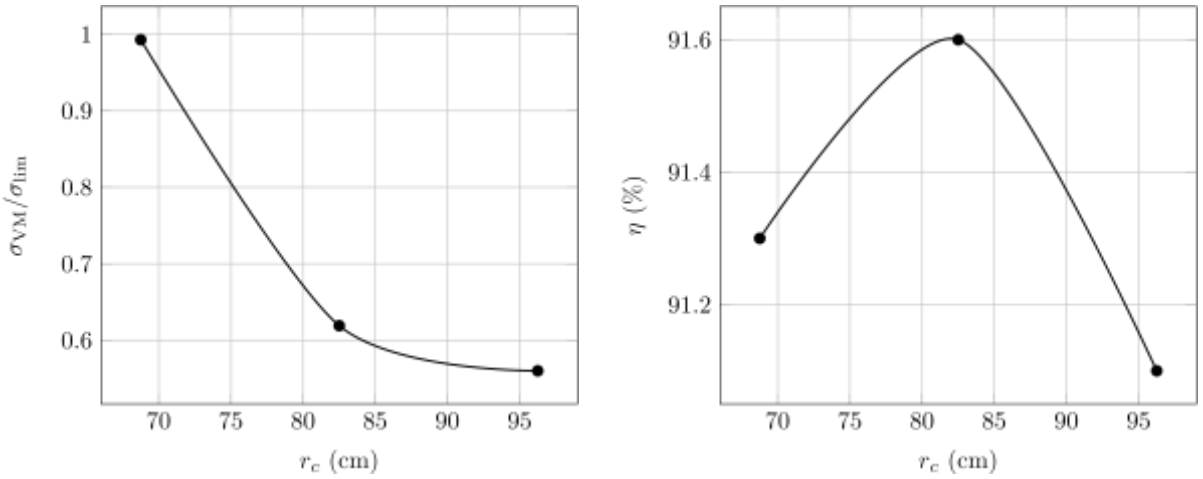

(a) Ratio of von Mises stress to ASME boiler code strength limit.

(b) Receiver thermal efficiency.

Figure 8: Sensitivity of receiver performance at the design point for various cavity radii (Receiver geometry: d_a=55 cm, h_c=123.75 cm).

Figure 9 presents the sensitivity of receiver performance at the design point for various aperture radii. The cavity radius and height were held constant at 82.5 cm and 123.75 cm, respectively. A receiver radius of 55 cm is seen to maximise both the thermal power output and receiver efficiency, confirming the result of the field optimisation study where a simplified model for receiver efficiency was used. Figure 10 and Figure 11 present a visual summary of the design point receiver thermal analysis results for optimal receiver geometry. The maximum solar irradiance on the receiver panels is approximately 1.1 MW/m^2, and is located near the heat transfer fluid inlets. Although it is more thermally efficient for a given flow path length to apply more heat towards the outlet than the inlet, the present flow path arrangement allows the length of piping to be minimised whilst keeping the pipe wall stress levels within its strength limit.

[1] The components of stress in the pipe wall due to temperature gradients are estimated by assuming a circumferentially uniform temperature distribution.

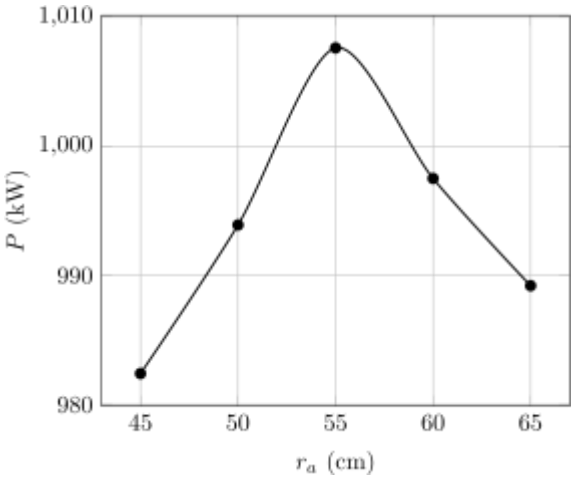

(a) Receiver thermal power output

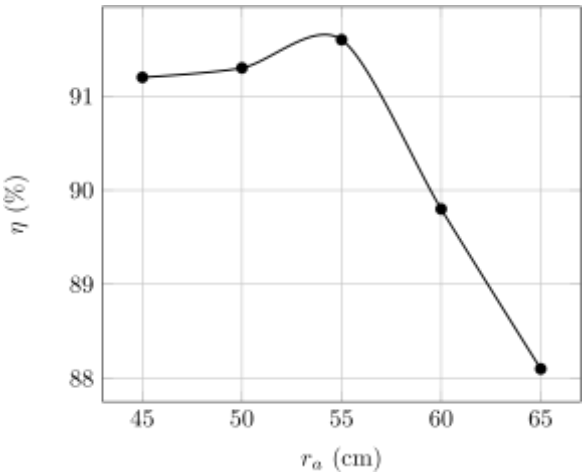

(b) Receiver thermal efficiency

Figure 9: Sensitivity of receiver performance at the design point for various aperture radii (Receiver geometry: r_c=82.5 cm, h_c=123.75 cm, Environment conditions: DNI=1002 W/m^2, wind = 1.6 m/s WNW, T_a=21°C).

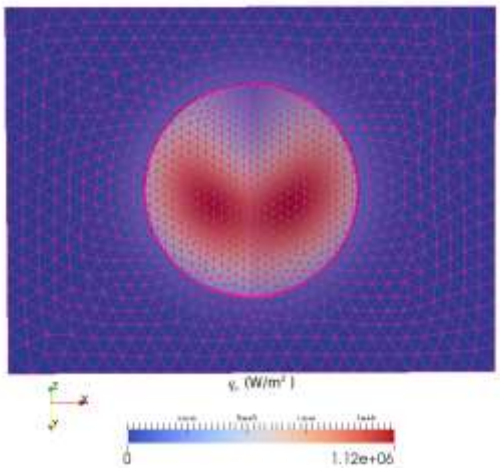

(a) Solar irradiance on all receiver parts with surface mesh shown.

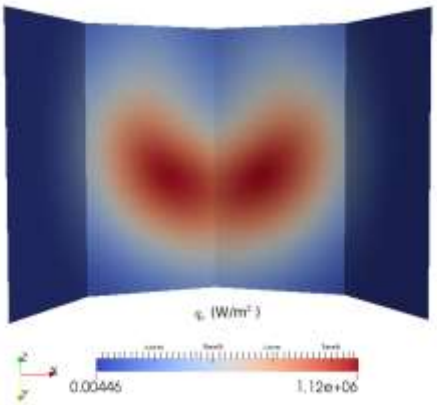

(b) Solar irradiance on the receiver panels.

Figure 10: Ray tracing results for solar noon on the Spring equinox (Receiver geometry: d_a=55 cm, r_c=82.5 cm, h_c=123.75 cm, Environment conditions: DNI=1002 W/m^2, wind = 1.6 m/s WNW, T_a=21°C).

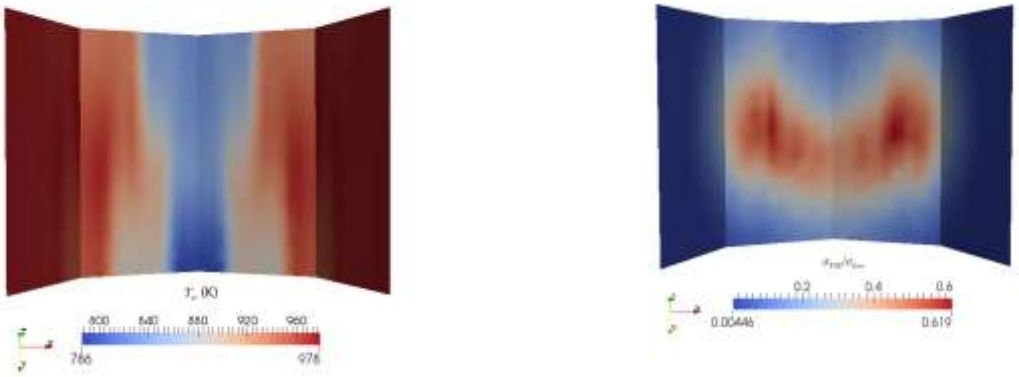

(a) Surface temperature on the receiver panels.

(b) Ratio of von Mises stress to material strength limit on the receiver panels.

Figure 11: Receiver thermal analysis results for solar noon on the Spring equinox (Receiver geometry: d_a=55 cm, r_c=82.5 cm, h_c=123.75 cm).

6. Conclusion

An integrated model for optical and heat transfer analysis of central receiver systems has been applied to optimise the heliostat field layout and receiver geometry for a 1 MW_t liquid sodium cavity receiver. A polar heliostat field with 413 heliostats combined with a 55 cm radius aperture orientated 60° down from the horizon was found to give an estimated annual thermal efficiency for the facility of 50.35%. Detailed heat transfer simulations of the receiver for a design point condition found an optimal cavity radius of 82.5 cm and confirmed the selection of a 55 cm radius aperture.

References

C.K. Ho, A.R. Mahoney, A. Ambrosini, M. Bencomo, A. Hall, and T.N. Lambert, 'Characterization of Pyromark 2500 Paint for High-Temperature Solar Receivers', 2013, *Journal of Solar Energy Engineering*, 136, p0145021-0145024.

J.-S. Kim, A. Burton, J. McGregor, W. Stein, and H. Nakatani, 'Design and test of a 600kWt receiver for solar air turbine systems', 2013, In *Proceedings of SolarPACES 2013 International Conference*.

M.F. Modest, 2013, 'Radiative Heat Transfer' (3rd ed.), *Academic Press*, London.

R.V. Padilla, Y.C. Soo Too, R. Benito, and W. Stein, 2015, 'Exergetic analysis of supercritical CO_2 Brayton cycles integrated with solar central receivers', *Applied Energy*, 148, p348-365.

C.A. Sleicher, and M.W. Rouse, 'A convenient correlation for heat transfer to constant and variable property fluids in turbulent pipe flow', 1975, *International Journal of Heat and Mass Transfer*, 18, p677–683.

S. Timoshenko, and J.N. Goodier, 1951, 'Theory of elasticity' (2nd ed.) *McGraw-Hill*, USA.

Acknowledgements

This work was performed as part of the ARENA sponsored *Optimisation of Central Receiver Systems for Advanced Power Cycles* project.